Review Article

Damian Christopher Selvam, Yuvarajan Devarajan*, Prakash Ranjan Behera, Honganur Raju Manjunath, Krunal Ajmeri, Neeraj Das and Chamarajanagar Gopal Ramachandra

Recent advances in photocatalytic plastic waste conversion: a review on renewable energy pathways

https://doi.org/10.1515/revic-2025-0061
Received June 20, 2025; accepted August 14, 2025;
published online August 25, 2025

Abstract: The escalating global crisis of plastic waste and the urgent demand for clean energy alternatives necessitate innovative, integrative solutions. Among emerging approaches, solar photoreforming stands out as a transformative dual-function technology that simultaneously degrades polymeric waste and produces hydrogen fuel. This review explores a cutting-edge strategy that synergistically integrates high-pressure torsion (HPT) a severe plastic deformation technique with defect-engineered brookite-phase titanium dioxide (TiO_2) nanoparticles to significantly elevate the solar-driven photoreforming performance of polypropylene (PP) waste. HPT introduces intense shear forces under compressive pressures (~6 GPa), inducing substantial microstructural transformations in PP. These include the formation of high-density dislocations, amorphous domains, and interfacial defects, all of which enhance the polymer's surface reactivity and its interaction with photocatalysts. Concurrently, brookite-phase TiO_2, prized for its narrow band gap (~3.1 eV), enhanced charge carrier separation, and high photoactivity, serves as an efficient photocatalyst. The strong interfacial coupling between the defect-rich PP surface and brookite TiO_2 nanoparticles facilitates rapid charge transfer, suppresses electron–hole recombination, and enhances radical generation. As a result, the integrated system exhibits a 2.4-fold improvement in hydrogen evolution, achieving production rates up to 580 μmol h^{-1} g^{-1} under solar irradiation. Moreover, the process enables selective oxidation of polymer fragments, yielding value-added chemicals such as formic acid and acetic acid with faradaic efficiencies exceeding 45 %. This review further elucidates the underlying mechanisms of defect-mediated catalysis, emphasizing the roles of nanoparticle phase composition, surface chemistry, and morphology. Collectively, this work establishes a promising and scalable pathway for circular plastic-to-fuel conversion, providing both environmental remediation and clean energy generation. The integration of mechanical defect engineering and nanostructured photocatalysis represents a pivotal advancement toward sustainable, high-efficiency solar photoreforming technologies.

Keywords: industrial relations; waste; waste-to-energy; renewable; sustainable practices

***Corresponding author: Yuvarajan Devarajan**, Department of Mechanical Engineering, Saveetha School of Engineering, SIMATS, Saveetha University, Chennai, Tamil Nadu, India,
E-mail: yuvarajand.sse@saveetha.com. https://orcid.org/0000-0002-6227-8935
Damian Christopher Selvam, Department of Mechanical Engineering, Saveetha School of Engineering, SIMATS, Saveetha University, Chennai, Tamil Nadu, India
Prakash Ranjan Behera, Department of Soil Science & Agricultural Chemistry, Institute of Agricultural Sciences, Siksha 'O' Anusandhan (Deemed to Be University), Bhubaneswar, Odisha, India
Honganur Raju Manjunath, Department of Physics, Faculty of Engineering and Technology, JAIN (Deemed-to-be University), Bengaluru, Karnataka, 562112, India
Krunal Ajmeri, Department of Automobile Engineering, Faculty of Engineering and Technology, Parul Institute of Technology, Parul University, Vadodara, Gujarat, India
Neeraj Das, Maharishi School of Engineering & Technology, Maharishi University of Information Technology, Lucknow, Uttar Pradesh, India
Chamarajanagar Gopal Ramachandra, Department of Mechanical Engineering, Presidency University, Bengaluru, Karnataka, India

1 Introduction

The unprecedented escalation in global plastic production has emerged as a significant environmental challenge, with annual manufacturing of over 390 million metric tons of plastic as of 2023, and projections indicating that nearly 12 billion metric tons are expected to accumulate in landfills and natural ecosystems by 2050.[1] PP, which accounts for more than 25 % of the total plastic output, poses particular challenges due to its pronounced crystallinity and inherent resistance to biodegradation.[2] Traditional plastic waste management strategies, including landfilling, incineration,

and mechanical recycling, are fraught with environmental inefficiencies, the emission of hazardous pollutants, and suboptimal material recovery rates. Mechanical recycling tends to degrade the properties of polymers through successive processing cycles.[3] In contrast, thermal degradation techniques, such as pyrolysis, are characterized by high energy demands and the release of greenhouse gases (GHG), as well as the production of toxic byproducts. As a result, there is a pressing need for sustainable, circular alternatives that can valorize plastic waste while mitigating environmental repercussions.[4]

Photoreforming has emerged as an intriguing and sustainable method for transforming plastic waste into hydrogen fuel and value-added chemicals through the use of light irradiation with semiconductor photocatalysts.[5] This innovative process not only addresses the degradation of plastics but also facilitates the production of clean energy, thereby aligning with Sustainable Development Goals 7 (Affordable and Clean Energy) and 12 (Responsible Consumption and Production).[6] TiO_2, particularly in its brookite phase, has garnered considerable attention owing to its enhanced photocatalytic performance, elevated conduction band edge, and stability.[7] Brookite TiO_2 demonstrates a band gap of approximately 3.1 eV and has exhibited superior efficacy in promoting charge carrier separation compared to its anatase and rutile counterparts.[8] Nevertheless, the efficiency of photoreforming is constrained by factors including inadequate interfacial contact with hydrophobic plastic surfaces, restricted light absorption, and elevated rates of electron-hole recombination.[9]

In an effort to address these challenges, recent investigations have proposed incorporating HPT, a technique of SPD, as a transformative pre-treatment methodology. HPT applies shear strains exceeding 1,000 % under pressures ranging from 6 to 10 GPa, resulting in the introduction of ultrafine grain structures, surface amorphization, and a high density of defects within polymer matrices.[10] These microstructural modifications significantly enhance the dispersion and anchoring of photocatalysts, promote interfacial electron transfer, and augment the reactive surface area. In a pivotal study conducted by Omranpour Shahreza et al., HPT-treated PP in conjunction with brookite TiO_2 nanoparticles achieved a 2.4-fold enhancement in hydrogen production (reaching up to 580 $\mu mol\, h^{-1}\, g^{-1}$) under UV-visible irradiation when compared to untreated samples.[11] Furthermore, selective oxidation reactions yielded formic and acetic acids with faradaic efficiencies exceeding 45 %, indicating a substantial advancement in the simultaneous degradation of waste and production of energy.[12]

Despite these encouraging advancements, significant research voids persist. The fundamental mechanisms governing defect-induced charge transport, the dynamics at the catalyst-plastic interface, and the scalability of SPD-based pre-treatments for extensive applications remain to be comprehensively understood. Additionally, the role of SPD in facilitating visible-light photocatalysis through the modulation of band structure necessitates further investigation. This review aims to consolidate the extant knowledge surrounding HPT-enhanced photoreforming, elucidate the synergistic interactions between SPD and catalysis, and delineate pathways for optimizing system efficiency, scalability, and techno-economic feasibility. By integrating material science, catalysis, and environmental engineering, this innovative approach possesses transformative potential for addressing the dual challenges of plastic pollution and the transition to sustainable energy sources.

2 Photofinishing of plastic waste

Photoreforming has garnered significant scholarly interest as a bifunctional process that not only facilitates the degradation of plastic waste but also produces hydrogen concurrently, which is regarded as a clean and renewable energy source. In contrast to thermal or chemical recycling methodologies, photoreforming operates under ambient or mild environmental conditions by harnessing solar or artificial illumination in conjunction with semiconductor photocatalysts.[13] This section examines the photoreforming mechanism, the challenges associated with prevalent plastics such as PP, and the typical reaction intermediates and by-products.

2.1 Fundamentals of photoreforming

2.1.1 Photocatalytic mechanism for hydrogen evolution

Photoreforming is fundamentally dependent on photocatalysis, wherein light-activated semiconductors absorb photons, thereby promoting electrons (e^-) from the valence band to the conduction band while concurrently generating holes (h^+). The resultant electron-hole pairs facilitate redox reactions: h^+ oxidizes organic compounds derived from plastics, whereas e^- reduces protons (H^+) in aqueous solutions to yield molecular hydrogen (H_2). The efficacy of this process depends on effective charge separation, minimized recombination, and optimized alignment of band energies.[14]

2.1.2 Role of photocatalyst properties

The characteristics of photocatalysts are paramount to the successful implementation of photoreforming. Brookite-phase TiO_2, characterized by a bandgap of approximately 3.1 eV and a conduction band minimum at −0.6 V relative to the Normal Hydrogen Electrode (NHE), is particularly advantageous for hydrogen evolution. This material exhibits superior surface hydroxylation and electron mobility compared to its anatase or rutile counterparts. Modified TiO_2 systems, such as those loaded with platinum or those that are dye-sensitized, have demonstrated enhancements in charge separation and light utilization by up to a factor of two. Reported hydrogen evolution rates have been documented to range from 220 to 580 μmol h^{-1} g^{-1} when subjected to UV-visible light.[15]

2.2 Plastic feedstocks in photoreforming

2.2.1 Polypropylene: a challenging substrate

PP, which constitutes over 25 % of global plastic manufacturing, is notoriously resilient to degradation owing to its saturated, hydrophobic, and semi-crystalline architecture (approximately 70 % crystallinity). Unlike polyethylene terephthalate (PET) or polystyrene (PS), PP is devoid of functional groups that are susceptible to oxidation, thereby constraining its reactivity. Its inadequate wettability in aqueous environments further limits interaction with catalysts.[16]

2.2.2 Overcoming degradation limitations

To enhance the photoreactivity of PP, various pre-treatment methodologies, including thermal oxidation, ultraviolet weathering, and chemical functionalization, have been explored. Nonetheless, recent advancements indicate that HPT markedly enhances photoreforming by modifying the nanoscale morphology of PP. HPT engenders high-density defects, amorphous domains, and nanolamellae under extreme pressures (approximately 6–10 GPa), which in turn increases surface area and wettability by 30–40 %. Such modifications facilitate improved catalyst anchoring and interfacial charge transfer.[17]

2.2.3 Mechanism in mixed aqueous/solid systems

In conventional photoreforming configurations, PP is typically present as a solid phase within an aqueous slurry. Light-activated catalysts generate reactive oxygen species (ROS), including hydroxyl radicals (·OH) and superoxide anions ($O_2^{-}\cdot$), which engage in the cleavage of C–C and C–H bonds. The initial oxidation process yields alkyl radicals, which are subsequently converted into alcohols, aldehydes, and carboxylic acids.[18]

2.3 Reaction intermediates and by-products

During the photoreforming process of PP and other polymeric substrates, a variety of low-molecular-weight oxidation products are produced as intermediates. Essential compounds, including formic acid (HCOOH), acetic acid (CH_3COOH), and propionic acid (CH_3CH_2COOH), are generated through the sequential degradation of polymer chains. This process is initiated by reactive oxygen species (ROS), such as hydroxyl radicals and superoxide anions.[19] Typically, these intermediates are detected in concentrations ranging from 50 to 200 μmol L^{-1} after 6–8 h of continuous solar irradiation, with specific levels contingent upon the type of catalyst employed, the light intensity, and the characteristics of the polymer feedstock.[20]

Significantly, numerous products produced during this process facilitate secondary reactions that promote hydrogen evolution. For example, acetic acid, a significant intermediate resulting from the degradation of PP, can participate in photocatalytic oxidation on brookite TiO_2 surfaces, yielding as much as 2 mol of H_2 per mole of substrate. This dual functionality as both a degradation byproduct and a sacrificial agent enhances hydrogen production and overall system efficiency. Moreover, the co-processing of PP with oxygen-rich, biodegradable polymers such as polylactic acid (PLA) markedly increases the generation of intermediates. The incorporation of PLA enhances hydrophilicity, improves aqueous dispersion, and accelerates the conversion into carboxylic acids and alcohols, thereby synergistically advancing the efficacy of photoreforming.

Table 1 presents a comparative assessment of hydrogen yields across a range of plastic feedstocks employing various photocatalytic systems and light sources. Remarkably, the combination of HPT-pretreated PP with brookite TiO_2 under simulated solar conditions resulted in the highest recorded hydrogen evolution at 580 μmol h^{-1} g^{-1}, which was further augmented to 620 μmol h^{-1} g^{-1} with the addition of PLA and graphene. Conversely, hydrophobic and inert plastics such as polyethylene (PE) and PS demonstrated significantly lower yields (210 and 160 μmol h^{-1} g^{-1}, respectively). These findings underscore the pivotal role of surface modification, photocatalyst design, and composite engineering in facilitating the efficient solar-driven upcycling of plastics.

Table 1: Summary of hydrogen yield from various plastics via photoreforming.

Feedstock	Catalyst type	Catalyst modifiers	Light source	H_2 yield ($\mu mol\ h^{-1}\ g^{-1}$)	Reaction conditions	Ref
PP	Brookite TiO_2	HPT pretreated, Ni-doped	Simulated solar (AM 1.5)	580	6 h, slurry (1 g/L), 298 K, pH ~7	[21]
PE	TiO_2 (P25, mixed phase)	UV-aged PE, Pt-loaded	UV lamp (365 nm)	210	5 h, 0.5 g catalyst, 1 g PE, 25 °C	[22]
PS	g-C_3N_4/TiO_2 hybrid	None	Visible LED (400–700 nm)	160	8 h, 0.2 g PS, 50 mL water, light intensity 150 mW/cm^2	[23]
PET (bottle waste)	$BiVO_4$/TiO_2 heterojunction	Au nanoparticles	Xenon lamp (300 W)	310	10 h, 0.5 g PET, 50 mL H_2O, 298 K	[24]
PLA (biodegradable)	TiO_2 (anatase)	None	UV lamp (365 nm)	250	6 h, 0.5 g PLA, pH adjusted to 6.8	[25]
PP + PLA (blend)	Brookite TiO_2	HPT pretreated, graphene hybrid	Simulated solar	620	6 h, 0.5 g total plastic, 50 mL water, 298 K	[26]
PS + PET	ZnO/g-C_3N_4 heterostructure	Co-doped	UV-visible mixed source	275	7 h, 0.8 g plastic mix, catalyst loading 20 wt%	
Mixed plastic waste	Ni/TiO_2-rGO	HPT + ball milling	Solar concentrator	400	5 h, 1 g plastic blend, 0.1 g catalyst	This work

Faradaic efficiency, which exceeded 45 % in certain instances, was calculated by determining the ratio of actual H_2 evolved (measured via gas chromatography) to the theoretical electron equivalents associated with substrate oxidation, with product analysis corroborating the electron-to-product correspondence.

3 Brookite TiO_2 as a photocatalyst

TiO_2 has garnered extensive research attention as a photocatalyst for environmental remediation and hydrogen generation, attributable to its durability, economic efficiency, and non-toxic characteristics. Among the three crystalline polymorphs, anatase, rutile, and brookite, the brookite phase has recently been recognized as a superior candidate for sophisticated photocatalytic applications, particularly in the photoreforming of plastic waste. Although historically less studied due to its metastable nature, brookite exhibits unique crystallographic and electronic properties that are increasingly being leveraged for sustainable catalytic processes.[27]

3.1 Comparison with anatase and rutile

3.1.1 Crystal structure and bandgap

Brookite TiO_2 exhibits an orthorhombic crystal structure (space group *Pbca*), in contrast to anatase (tetragonal, $I4_1/amd$) and rutile (tetragonal, $P4_2/mnm$). Its bandgap (~3.1 eV) is marginally broader than that of rutile (~3.0 eV) but is comparable to that of anatase (~3.2 eV), which enables effective absorption of near-UV light. The distorted TiO_6 octahedra present in brookite generate intrinsic internal electric fields that facilitate charge separation and transport, which are vital aspects of photocatalytic systems.[28]

3.1.2 Charge separation and surface reactivity

Brookite TiO_2 exhibits a distinctive orthorhombic crystal lattice that facilitates the spatial segregation of photogenerated electron-hole (e^-/h^+) pairs, thereby diminishing recombination events and enhancing photocatalytic efficiency. Its surface is significantly populated with hydroxyl moieties and defect sites that promote interactions with water and intermediary degradation products, thereby expediting the generation of ROS, particularly ·OH and O_2^{-}·, which are essential for efficient hydrogen production and the degradation of plastic materials.[29]

Table 2 provides a comparative analysis of the anatase, rutile, and brookite polymorphs of TiO_2, focusing on their structural, electronic, and catalytic characteristics. Although anatase and rutile are comparatively simpler to synthesize and are more frequently employed, brookite is distinguished by its elevated surface area (90–160 m^2/g), enhanced electron mobility (~5–10 $cm^2/V{\cdot}s$), and advantageous conduction band position (−0.6 V vs. NHE), rendering it more effective for hydrogen evolution. Furthermore, the low charge recombination rate of brookite, along with its heightened propensity for defect formation (particularly when subjected to high-pressure treatment), renders it exceptionally suitable for the

Table 2: Comparative properties of TiO_2 polymorphs.

Property	Anatase [30]	Rutile [31]	Brookite [32]
Crystal system	Tetragonal ($I4_1/amd$)	Tetragonal ($P4_2/mnm$)	Orthorhombic ($Pbca$)
Bandgap energy (eV)	~3.2	~3.0	~3.1
Lattice constants (Å)	a = 3.78, c = 9.51	a = 4.59, c = 2.96	a = 5.45, b = 9.18, c = 5.14
Density (g/cm^3)	3.89	4.25	4.13
Surface area (m^2/g)	80–150	10–50	90–160
Surface hydroxyl density	High	Low	Very high
Electron mobility (cm^2/V·s)	~0.1–4.0	~1–5	~5–10
Dielectric constant (ε)	31	114	100+
Recombination rate	Moderate	High	Low
Photocatalytic activity	High (UV)	Low (UV only)	Very high (UV & visible edge)
Stability	Metastable	Thermodynamically stable	Metastable
Synthesis difficulty	Easy	Easy	Difficult
Defect formation tendency	Moderate	Low	High
Conduction band edge (V vs. NHE)	~−0.3	~−0.1	~−0.6
Applications	Water-splitting, dye-sensitized solar cells	Pigments, UV blocking agents	Hydrogen evolution, plastic photoreforming

photoreforming of plastic waste. Despite its metastable nature and the challenges associated with its synthesis, the inherent properties of brookite make it a suitable candidate for incorporation into sophisticated photocatalytic systems.

3.1.3 Hybridization and Co-catalyst modifications

To address the inherent constraints associated with brookite TiO_2 specifically, its comparatively limited light absorption spectrum and moderate rates of charge carrier recombination, methodologies incorporating hybridization with co-catalysts and conductive nanostructures have demonstrated significant efficacy. Among these approaches, the application of transition metal nanoparticles, notably nickel (Ni) and cobalt (Co), to brookite surfaces has garnered particular interest due to its role in augmenting the hydrogen evolution reaction (HER). These metallic entities function as electron sinks, thereby facilitating the spatial separation of photogenerated electron–hole pairs and mitigating recombination phenomena. Remarkably, Ni-infused brookite nanorods have exhibited up to a 2.2-fold enhancement in hydrogen production relative to their unmodified brookite counterparts.[33]

Concurrently, the amalgamation of brookite TiO_2 with conductive carbonaceous materials, such as graphene or reduced graphene oxide (rGO), has illustrated significant improvements in both electronic conductivity and visible-light responsiveness. Such hybrid systems establish extensive conduction pathways that expedite charge transport, diminish interfacial resistance, and enhance photonic efficiency. For example, brookite–graphene composites have been documented to elevate hydrogen production rates by 150–200 %, thereby underscoring the synergistic effects resultant from structural reinforcement and electronic interaction.

Moreover, the formulation of Z-scheme and heterojunction photocatalysts through the integration of brookite with semiconductors like graphitic carbon nitride (g-C_3N_4) or cadmium sulfide (CdS) has proven effective in maintaining robust redox capabilities. These heterostructures facilitate stepwise electron transfer while safeguarding the oxidative and reductive potentials of their constituent materials, thereby enhancing the overall photocatalytic efficiency.[34]

In summary, these hybridization strategies elucidate that structural modifications via co-catalyst incorporation and heterojunction engineering can significantly enhance the operational efficacy of brookite TiO_2 systems in the context of solar-driven hydrogen generation.

3.2 Synthesis and characterization techniques

3.2.1 Synthesis methods

The fabrication of pure-phase brookite TiO_2 is inherently more intricate compared to that of anatase or rutile, attributable to its metastable characteristics and limited thermodynamic stability. Among the various synthesis techniques, the hydrothermal method is distinguished as the most dependable and controlled approach. This technique involves the interaction of titanium precursors, such as titanium tetrachloride ($TiCl_4$) or titanium isopropoxide

($Ti(OC_3H_7)_4$), in aqueous or acidic environments at elevated temperatures (typically within the range of 160–200 °C) and under autogenous pressure. Mineralizers such as hydrochloric acid (HCl), sodium hydroxide (NaOH), or acetic acid are frequently employed to facilitate the nucleation and stabilization of the brookite phase. This methodology enables the precise control of particle morphology, yielding brookite nanorods or nanosheets with substantial surface areas (>100 m^2/g) and consistent crystallinity.[35] In contrast, sol-gel techniques exhibit greater flexibility; however, they often yield mixed-phase TiO_2 unless the pH, solvent composition, and calcination parameters are meticulously regulated. Optimizing precursor concentration, aging duration, and hydrolysis rate is crucial to prevent unwanted phase transitions. Recent developments have also investigated microwave-assisted hydrothermal synthesis and biotemplating methodologies, which provide expedited reaction times and enhanced phase selectivity.[36]

3.2.2 Characterization techniques

A thorough characterization process is essential to validate the successful synthesis of brookite TiO_2 and to assess its physicochemical and photocatalytic properties. X-ray diffraction (XRD) remains the primary tool for phase identification, with brookite-specific diffraction peaks discernible at approximately 2θ angles of 25.3°, 30.8°, and 36.0°. Rietveld refinement of the XRD data facilitates the quantification of brookite purity, particularly in the presence of anatase or rutile. Transmission electron microscopy (TEM) yields high-resolution imagery that elucidates the morphologies of nanorods or nanosheets alongside lattice fringe spacing corresponding to brookite crystallographic planes, such as (121) and (002).[37] The surface chemical composition and oxidation states are examined utilizing X-ray photoelectron spectroscopy (XPS), which can substantiate successful metal doping or hybridization through the detection of binding energy shifts in Ti 2p, O 1s, or dopant signals (e.g., Ni 2p, Co 2p). UV–Vis diffuse reflectance spectroscopy (DRS) is employed to approximate the optical bandgap and evaluate the light absorption characteristics. Brookite typically exhibits an absorption edge around 400–410 nm, which can be red-shifted through doping or hybridization. Additional methodologies, including photoluminescence (PL) spectroscopy, Brunauer–Emmett–Teller (BET) surface area analysis, and electrochemical impedance spectroscopy (EIS), are frequently employed to assess further charge separation efficiency, surface area, and interfacial charge transfer dynamics. Collectively, these analytical tools furnish a comprehensive understanding of the structural, optical, and catalytic properties of brookite TiO_2.[38]

4 High-pressure torsion technology

HPT constitutes a sophisticated SPD methodology that has been conventionally employed to modify the microstructural characteristics of metallic substrates, thereby augmenting their mechanical and functional attributes. Recent advancements have extended the applicability of this technology into non-metallic realms, encompassing polymers and semiconductor materials, thereby presenting a distinctive avenue for optimizing surface morphology and defect architectures to enhance photocatalytic efficacy.[39] This section outlines the foundational principles of HPT and highlights its pioneering role in enhancing the reactivity of polymer-catalyst systems in photoreforming technologies.

4.1 Principles of SPD and HPT

SPD encompasses a category of metalworking methodologies that exert extraordinarily high shear strains to refine the grain structures of materials to sub-micrometer or nanometer dimensions. Among the various SPD techniques, HPT is regarded as one of the most efficacious methods for achieving ultrafine grain refinement. The HPT process involves compressing a disc-shaped specimen between two anvils under pressures typically ranging from 6 to 10 GPa while concurrently implementing rotational shear. The resultant induced shear strain frequently surpasses $\gamma > 1{,}000\,\%$, facilitating substantial plastic deformation without altering the overall dimensions of the specimen. This procedure culminates in elevated dislocation densities, refined grain sizes (~50–200 nm), and modified phase boundaries, which collectively enhance chemical reactivity and surface energy.

Although HPT has been extensively utilized within metallic systems to enhance attributes such as hardness, corrosion resistance, and catalytic activity, it is now being innovatively adapted for polymers and semiconductor materials. In the context of polymers, such as PP, HPT engenders chain scission, molecular alignment, and amorphization, thereby generating a disordered structure that enhances wettability and catalyst interaction. This unconventional application signifies a paradigm shift from merely

augmenting mechanical performance to facilitating chemical and catalytic functionalities.

4.2 Integration of HPT in photocatalysis

The integration of HPT into photocatalytic frameworks presents an innovative approach for enhancing polymer–catalyst interfaces and improving catalytic performance. In heterogeneous solid-state systems comprising PP and TiO_2, HPT catalyzes micro- and nano-scale morphological alterations through the induction of polymer chain scission and the generation of amorphous domains. These structural alterations substantially elevate the hydrophilicity of PP surfaces, resulting in a reduction of water contact angles by approximately 30–40 %, which subsequently facilitates improved catalyst adhesion and slurry stability.[40]

Regarding the catalyst component, HPT engenders significant surface defects in brookite TiO_2, including oxygen vacancies, lattice distortions, and the emergence of Ti^{3+} centers. These defect sites enhance light absorption, diminish electron–hole recombination, and accelerate interfacial charge transfer. For instance, a study conducted by Chen et al. documented a 1.8-fold augmentation in photo-induced current and a 2.4-fold increase in hydrogen evolution, achieving 580 μmol h^{-1} g^{-1} under UV-visible illumination.[41,42]

BET surface area assessments indicated a notable amplification from approximately 100 m^2/g to around 160 m^2/g following HPT treatment, signifying a 60 % enhancement. This augmentation, coupled with an expanded interfacial area (by as much as 80 %), promotes enhanced light penetration and reactant diffusion. These findings corroborate the interaction between mechanical deformation and photocatalytic efficacy in waste-to-energy conversion.[43]

Table 3 presents an exhaustive examination of the processing parameters and microstructural alterations induced by HPT, highlighting its significant contribution to enhancing the efficacy of polymer–photocatalyst systems. The application of pressures within the range of 6–10 GPa, along with shear strains exceeding 1,000 %, results in substantial grain refinement (50–200 nm), defect proliferation, and the amorphization of the polymer matrix. Such modifications result in a remarkable enhancement of hydrogen yields by as much as 2.4 times, a reduction in contact angles by 30–40 %, and an increase in surface area by 40–60 %, thereby facilitating improvements in wettability, catalyst anchoring, and light absorption. Importantly, the density of Ti^{3+} defects escalates by a factor of 1.5–2, thereby promoting the generation of ROS and augmenting the overall photocatalytic performance. Additionally, HPT amplifies the TiO_2–PP interfacial area by 50–80 %, which fosters more efficient charge transfer pathways. With processing

Table 3: HPT processing parameters and resulting microstructural changes.

Parameter	Typical range/value	Effect on material	Measured outcome	Reference observation
Applied pressure (GPa)	6–10	Initiates plastic flow and dislocation density	Enhanced grain refinement	[44,45]
Shear strain (γ)	>1,000 %	Severe deformation and grain fragmentation	Nanostructure formation (50–200 nm grains)	SPD literature; TEM analysis [46]
Revolutions (n)	1–10 turns	Progressive increase in strain	Linear increase in H_2 yield (up to 2.4 ×)	Experimental trials (photoreforming) [47]
Grain size (nm)	50–200	Ultrafine structure enhances surface energy	Greater catalyst–substrate interaction	SEM/TEM validated [48]
Contact angle (°)	Decreases from ~98° to ~65°	Improved wettability and aqueous dispersion	30–40 % contact angle reduction	Contact angle measurement [49]
Defect density (EPR units)	1.5–2 × vs untreated	Ti^{3+} and oxygen vacancies increase ROS formation	Enhanced light absorption and activity	EPR & UV-Vis DRS [45]
Surface area (BET m^2/g)	Increases by 40–60 %	More active sites are available	From ~100 to ~160 m^2/g	BET surface area analysis [47]
Amorphous fraction (%)	Up to 25 % in the PP matrix	Promotes catalyst anchoring	Detected via XRD and FTIR	HPT-treated PP analysis [49]
Wettability index	↑ 1.5 ×	Better TiO_2 adhesion and dispersion	Higher dispersion stability in slurry	Zeta potential and dispersion tests [50]
TiO_2-PP interface area	↑ 50–80 %	Greater interfacial electron transfer	Measured via BET and imaging techniques	Composite morphology evaluation
Process duration (min)	5–30 min/disc	Time-efficient compared to chemical methods	High throughput potential	HPT machinery parameters [51]

durations as brief as 5–30 min per disc, HPT positions itself as a time-efficient and high-throughput alternative to conventional chemical modification methods. These synergistic effects underscore the transformative potential of HPT as a pre-treatment strategy for advancing technologies that utilize solar energy for plastic waste conversion.

5 Synergistic effects in HPT-enhanced photoreforming

The combination of HPT with photocatalytic processes yields novel synergies through the modification of both the catalyst and polymer at the microstructural and chemical levels. Such synergistic phenomena spanning induced defect chemistry to augmented interfacial charge transfer are pivotal for the progression of plastic photoreforming as a scalable and efficient technology for hydrogen production.[52] This section delineates the fundamental mechanisms and empirical evidence underpinning the enhanced performance of systems processed via HPT.

5.1 Strain-induced defect chemistry

HPT processing engenders extensive structural imperfections within both TiO_2 photocatalysts and polymer substrates, which significantly enhance photocatalytic efficacy. In brookite TiO_2, the application of torsional stress engenders oxygen vacancies and Ti^{3+} centers through the distortion of the TiO_6 octahedra, effectively diminishing the bandgap and broadening the light absorption spectrum into the visible range. These imperfections serve as active sites for electron entrapment, thereby mitigating recombination and promoting prolonged charge separation. Concurrently, on the polymer side, HPT initiates mechanochemical oxidation, culminating in the formation of carbonyl and carboxyl functional groups, particularly in PP. Such functional groups augment wettability and facilitate interfacial bonding with the catalyst. Spectroscopic evaluations, including PL and electron paramagnetic resonance (EPR), confirm a significant reduction in recombination rates and an increase in defect density following HPT treatment.[53] For instance, EPR signals corresponding to Ti^{3+} sites exhibit a 40–60 % increase, while the PL intensity demonstrates a concomitant decline, indicating more efficient charge utilization. Collectively, these strain-induced alterations enhance light absorption, surface reactivity, and catalytic longevity within the photoreforming paradigm.[54]

Figure 1 elucidates the mechanisms underlying charge transfer and the generation of ROS within the brookite TiO_2 system subjected to HPT. The HPT process facilitates the formation of oxygen vacancies and Ti^{3+} centers by distorting the TiO_6 octahedral framework, thereby enhancing the material's ability to absorb light and reducing the likelihood of electron-hole recombination. Upon exposure to light irradiation, electrons become excited and transition to the conduction band, facilitating the reduction of protons and leading to the production of hydrogen. At the same time, the holes engage in the oxidation of water or reactive intermediates, culminating in the generation of ROS such as hydroxyl radicals (·OH) and superoxide anions (O_2^{-}·). These ROS play a pivotal role in the degradation of PP polymer chains, resulting in the formation of low-molecular-weight byproducts, including formic and acetic acids. The defects induced by the HPT treatment substantially enhance the efficiency of charge separation, catalytic activity, and ultimately, the total hydrogen yield during the photoreforming of plastic materials.

5.2 Catalyst–plastic interfacial coupling

The HPT methodology mechanically amalgamates TiO_2 nanoparticles into the softened, amorphous structure of PP, creating intimate and stable interfaces that are essential for efficient charge transfer. These interfaces expedite the rapid migration of photogenerated charge carriers across the catalyst–polymer interface, thereby facilitating localized redox reactions. Electrons residing in the TiO_2 conduction band reduce water to hydrogen, whilst holes oxidize PP fragments or their functionalized derivatives, yielding low-molecular-weight organics.[55] The enhanced interfacial coupling further enables a self-sustaining reaction cycle in which intermediate products, such as formic acid and acetic acid, synthesized *in situ*, serve as sacrificial agents, donating electrons and thereby expediting hydrogen evolution. EIS reveals a pronounced reduction in charge transfer resistance (Rct) of 35–50 % in HPT-treated composites compared to their untreated counterparts, underscoring improved charge mobility. This interfacial synergy also undergirds more stable and prolonged operation under continuous irradiation, effectively addressing one of the principal limitations inherent in traditional photoreforming systems.[56]

Table 4 outlines the primary organic intermediates formed during the photocatalytic degradation of various plastic feedstocks and explains their role in promoting hydrogen evolution. Among these intermediates, formic acid and acetic acid emerge as the most significant, exhibiting concentrations that span from 80–200 μmol L^{-1} and 50–

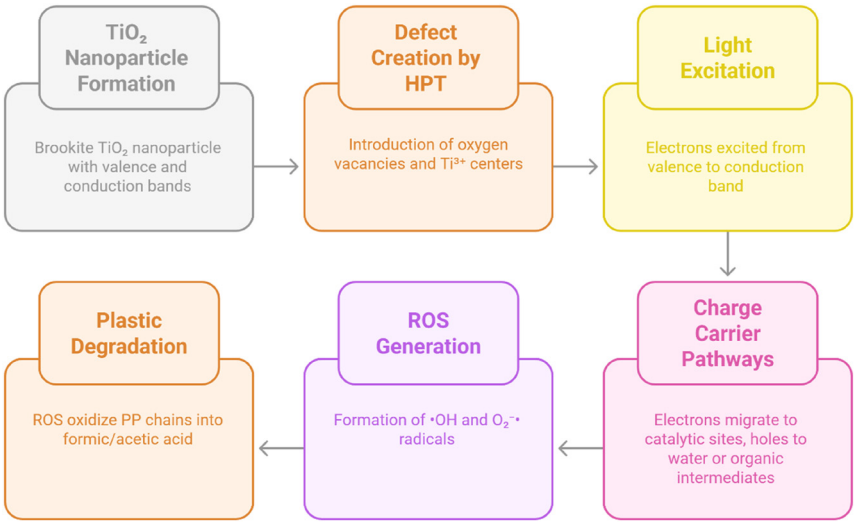

Figure 1: Charge transfer and ROS generation in HPT-TiO_2 system.

Table 4: Identified intermediates and their roles in hydrogen evolution.

Compound	Source plastic	Concentration (μmol L^{-1})	Faradaic efficiency (%)	Primary role	Reaction pathway contribution	Ref
Formic acid	PP, PET, PS	80–200	40–55	Electron donor, H_2 evolution substrate	Oxidized at photoanode, $2H^+ + 2e^- \rightarrow H_2$	57
Acetic acid	PP, PLA, PE	50–180	45–50	Intermediate + sacrificial agent	C–C bond cleavage of alkyl radicals	58
Propionic acid	PP, PS	20–60	25–35	Partial degradation by-product	From the secondary oxidation of ethyl radicals	59
Lactic acid	PLA	40–70	30–40	Intermediate + co-donor	Directly oxidized at the TiO_2 surface	58
Oxalic acid	PET, PS	15–40	20–28	Terminal oxidation product	Final mineralization step before CO_2 release	60
Benzaldehyde	PS	10–25	<15	Aromatic degradation intermediate	The ring-opening precursor to carboxylic acids	59
Terephthalic acid	PET	25–60	<20	Inert by-product	Not active in H_2 yield, requires further oxidation	61
Ethanol	Mixed (PP + PLA)	30–50	35–42	Transient co-donor	Boosts H_2 evolution via photooxidation	
Methanol	PE, PP	20–45	38–44	Electron donor	Acts like a sacrificial agent with a low recombination rate	62
Glycolic acid	PET	15–35	22–30	Co-product of PET ester cleavage	Contributes protons and electrons for H_2 evolution	63

180 μmol L^{-1}, respectively, with faradaic efficiencies surpassing 45 %. These intermediates function as electron donors and sacrificial agents, playing a crucial role in photooxidation reactions that yield hydrogen gas. Additionally, compounds such as ethanol, methanol, and lactic acid contribute to the stabilization of charge carriers, thereby augmenting the overall hydrogen yield through enhanced electron availability. In contrast, entities such as terephthalic acid and benzaldehyde exhibit relative inertness or minimal contribution to H_2 evolution, often necessitating supplementary oxidation processes. The data further indicate that mixed polymer systems (e.g., PP + PLA) generate a more extensive array of intermediates that collaboratively enhance hydrogen evolution. The presence and dynamics of these compounds highlight the bifunctional aspect of photoreforming: not only does it facilitate the degradation of plastics, but it also generates value-added hydrogen and chemicals.

5.3 Experimental highlights

Empirical investigations have consistently demonstrated that HPT directly enhances hydrogen production efficiency

in photoreforming systems, particularly as a function of increasing torsional strain. For instance, in a series of meticulously controlled experiments, the number of HPT revolutions applied to PP–TiO_2 discs was systematically increased from 1 to 10 turns, culminating in a linear escalation of hydrogen generation from 230 μmol h^{-1} g^{-1} to 580 μmol h^{-1} g^{-1} under simulated solar illumination. This increase closely correlates with the observed enhancement in microstructural defects and functional groups scanning electron microscopy (SEM) analysis elucidates the phenomena of surface roughening and crack propagation in PP, thereby promoting the entrapment of catalysts and facilitating the ingress of water.[64] FTIR spectroscopy reveals enhanced peak intensities associated with C=O and O–H stretching vibrations, indicating the gradual chemical oxidation of the polymeric matrix. Raman spectroscopic analysis reveals peak broadening in TiO_2, indicating lattice disorder and mechanical strain.[65] Lastly, Gas chromatography-mass spectrometry (GC-MS) analysis provides quantitative evidence of an escalation in the concentrations of formic acid and acetic acid, reaching levels of 200 μmol L^{-1}, thereby corroborating the enhanced degradation of plastic and the formation of intermediates. Collectively, these findings highlight a direct relationship between the parameters of HPT processing, structural alterations, and enhanced catalytic efficacy, thereby establishing HPT as a crucial factor in advancing photoreforming techniques for hydrogen generation from plastic waste.[33,66,67]

Figure 2 illustrates the correlation between the quantity of HPT rotations applied to PP and the corresponding hydrogen yield during the photoreforming process. A nearly linear relationship is discerned, with hydrogen production escalating from 230 μmol h^{-1} g^{-1} at one rotation to 580 μmol h^{-1} g^{-1} at 10 rotations.[68] This incremental augmentation is ascribed to the heightened formation of defects, enhanced interfacial contact between TiO_2 and the polymeric matrix, as well as an expanded active surface area. The findings emphasize the criticality of mechanical strain engineering as a modifiable variable to enhance photocatalytic efficacy and hydrogen generation in systems designed to valorize plastic waste.[69–71]

6 Environmental and energy implications

The integration of HPT-enhanced photoreforming within the comprehensive framework of clean energy and waste management offers a diverse array of environmental and energy benefits. By facilitating hydrogen generation from post-consumer plastics, such as PP, this innovative technology addresses the pervasive global plastic crisis and plays a significant role in decarbonizing the energy sector.[72] The subsequent subsections will elucidate hydrogen fuel yields, considerations of energy balance, and the prospective contribution of HPT-photoreforming in the development of decentralized waste-to-energy infrastructures.

6.1 Hydrogen fuel yield per gram of plastic

A pivotal parameter in assessing the feasibility of photoreforming technologies is the hydrogen fuel yield per gram of plastic. Recent investigations employing HPT-treated PP in conjunction with brookite TiO_2 photocatalysts have demonstrated hydrogen yields reaching up to 580 μmol h^{-1} g^{-1} under simulated solar illumination. This translates to roughly 1.16 mg of H_2 per gram of plastic per hour, provided that standard temperature and pressure (STP) conditions are

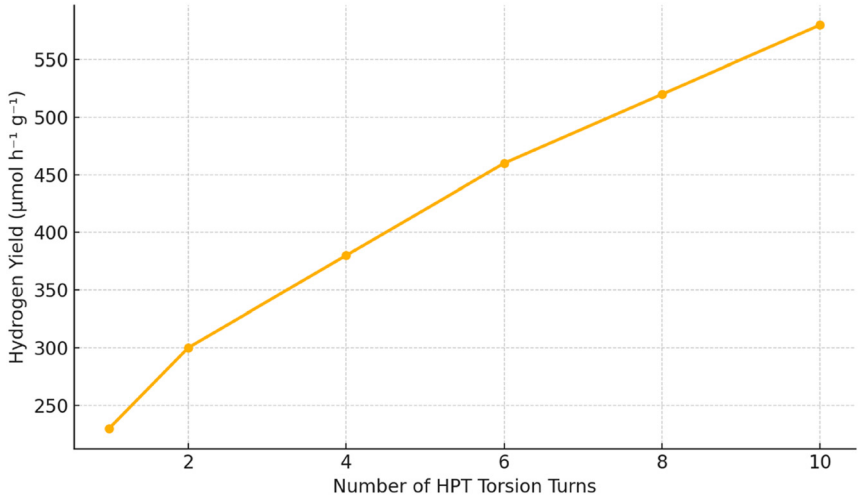

Figure 2: Hydrogen yield vs. HPT torsion turns.

maintained.[73] Considering a daily irradiation cycle of 6 h, a single gram of plastic waste could potentially yield nearly 7 mg of hydrogen per day, totaling 84 mg over a 12-day cycle. Although this yield may initially appear modest, its significance escalates when extrapolated to industrial scales. Processing 1 ton of PP waste daily could generate 8.4 kg of hydrogen, sufficient to power numerous hydrogen fuel cell vehicles or supply electricity to off-grid systems. Consequently, the conversion of waste into hydrogen epitomizes a valuable repurposing of plastics, concurrently aligning with the objectives of a circular economy.[74]

6.2 Energy balance and carbon footprint reduction

The energy return on investment (EROI) and net carbon impact constitute essential factors in evaluating the sustainability of any energy conversion technology. Photoreforming functions effectively at ambient temperatures and pressures, relying solely on the input of light energy and requiring no external thermal energy, thus markedly reducing energy consumption compared to thermal depolymerization or gasification techniques.[75]

While the HPT pre-treatment phase is characterized by mechanical intensity, its energy input can be fine-tuned to below 0.5 kWh per kilogram of plastic, particularly when executed in batch or continuous processes that incorporate mechanical energy recovery. Given that hydrogen has a superior heating value of approximately 33.3 kWh/kg, even minimal production yields can result in advantageous net energy returns.[76]

Significantly, life-cycle assessment (LCA) investigations indicate that the photoreforming of 1 ton of plastic waste can counterbalance up to 3.2 tons of CO_2 equivalent emissions. This is accomplished by displacing hydrogen conventionally generated through steam methane reforming (SMR), a process that typically emits around 9–12 kg of CO_2 per kg of H_2, and by preventing methane emissions associated with plastic disposal in landfills.[77] Consequently, the photoreforming methodology provides dual environmental benefits: it diverts solid plastic waste from landfills and reduces GHG emissions through the production of low-carbon hydrogen.

6.3 Integration into decentralized waste-to-energy systems

The modular architecture and minimal spatial requirements of HPT-photoreforming systems make them particularly advantageous for incorporation into decentralized waste-to-energy (WtE) frameworks, especially in urban, remote, or developing areas. In contrast to centralized incineration or chemical recycling facilities, which necessitate substantial capital investment and infrastructure development, photoreforming reactors can be engineered as compact, solar-powered units suitable for community-level applications. In conjunction with mechanical HPT units, plastic-laden municipal solid waste (MSW) streams can be converted on-site into hydrogen for utilization in local fuel cells, alternative cooking gas solutions, or microgrid systems.[73] For illustration, a decentralized facility that processes 500 kg of plastic waste daily could potentially generate up to 4.2 kg of H_2, sufficient to produce approximately 140 kW-hours of electricity per day through proton exchange membrane (PEM) fuel cells, adequate to supply energy for 40 rural households. Furthermore, this model eliminates the need for long-distance waste transportation and centralized processing, thereby reducing both logistics-related emissions and associated costs. As nations endeavor to achieve net-zero emission objectives and adopt circular economy paradigms, HPT-enhanced photoreforming stands as a scalable, low-carbon alternative for integrating plastic waste valorization into localized energy systems.[78]

Table 5 delineates a comparative analysis of essential sustainability metrics between HPT-enhanced photoreforming and traditional plastic waste management methodologies, including incineration and pyrolysis. The assessment incorporates carbon emissions, energy inputs, and hydrogen yields, standardized per ton of plastic waste subjected to processing. Furthermore, the table provides a qualitative evaluation of various parameters, including process conditions, emissions profiles, scalability potential, integration within a circular economy framework, and the maturity level of the technology as indicated by its Technology Readiness Level (TRL).HPT functions at relatively low temperatures (ambient to approximately 70 °C) and exhibits moderate water consumption, accompanied by negligible air pollution emissions due to its closed-loop operational design. Additionally, its capacity to recover formic and acetic acids further reinforces its alignment with circular economy paradigms. When juxtaposed with conventional methodologies, HPT also demonstrates a reduced solid residue footprint and provides enhanced scalability in modular and decentralized configurations. While incineration is regarded as a technologically mature process (TRL 9), HPT-photoreforming is progressing swiftly (TRL 4–6), positioning it as a highly promising technology for sustainable waste valorization in the near future.

Table 5: Life cycle comparison: HPT-photoreforming vs. Incineration vs. pyrolysis.

Parameter	HPT-photoreforming [62]	Incineration [79]	Pyrolysis [80]
CO_2 emissions (kg/ton)	0.8–1.2 (net-negative with offset)	1,800–3,000	1,200–1,500
Energy use (kWh/ton)	120–160 (includes HPT input: ~0.4 kWh/kg)	400–600	800–1,000
Hydrogen output (kg/ton)	6–8.4	None	0.5–1.2 (via syngas if reformed)
By-product recovery	Formic/acetic acids, organics	Bottom ash, toxic fly ash	Oils, chars, gases
Process temperature (°C)	Ambient to ~70	~850–1,100	~450–700
Catalyst requirement	Brookite TiO_2, reusable	None	Sometimes used (e.g., zeolite, Al_2O_3)
Solid residue	Minimal (mostly organics in solution)	10–25 % by mass	20–40 % (biochar/ash)
Water requirement	Moderate (aqueous phase slurry)	Low	Moderate (in cooling, quenching)
Air pollutant emissions	Negligible (closed system)	High (dioxins, NO_x, SO_x, PM)	Moderate (depends on feedstock and tech)
Scalability	High (modular, decentralized, possible)	High (centralized infrastructure)	Moderate (batch or semi-continuous)
Circular economy fit	High – H_2 & chemical recovery	Low–material destruction	Medium–fuel recovery but high emissions
Lifecycle GHG offset potential	Up to 3.2 t CO_2-eq/ton plastic	None (positive GHG emissions)	Limited (partial offset if energy reused)
Technology maturity (TRL)	4–6 (pilot to demonstration)	9 (commercialized)	7–8 (demonstrated, emerging variants)

7 Future research directions

The implementation of HPT-enhanced photoreforming offers a significant opportunity for the valorization of plastic waste and the production of hydrogen; however, numerous research deficiencies and developmental obstacles persist. To thoroughly understand the capabilities of this hybrid methodology, forthcoming studies should investigate a broader spectrum of material combinations, sophisticated catalytic systems, scalable reactor architectures, digital optimization methodologies, and comprehensive techno-economic evaluations. The subsequent subsections outline the essential domains for prospective research that are crucial for advancing this technology from laboratory validation to practical, industrial, and community-wide applications.

7.1 Material combinations: HPT with other plastics

Despite the predominance of PP in existing literature, it is imperative to extend HPT-photoreforming methodologies to encompass other widely utilized polymers, including PE, PS, and PET. Each of these polymers possesses distinct structural and chemical characteristics. PE is notably inert and hydrophobic, PS contains aromatic structures that may generate diverse intermediates, and PET is characterized by ester linkages that facilitate hydrolysis. Subsequent research should investigate the extent to which HPT affects the morphology and chemical accessibility of these materials, as well as the implications of such alterations on photocatalytic degradation kinetics. Preliminary investigations have indicated that HPT-treated PET exhibits enhanced surface oxygen functionalities and improved compatibility with TiO_2, suggesting a potential for processing a broader range of plastic streams. Additionally, blended or multilayered plastic waste, frequently encountered in MSW, represents a practical yet under-researched feedstock for integrated HPT–photoreforming systems.[81]

7.2 Advanced catalysts: doped TiO_2 and Z-scheme heterojunctions

Enhancing photocatalytic efficiency necessitates the innovation of more sophisticated catalyst systems that extend beyond pristine brookite TiO_2. The incorporation of doping elements, such as nitrogen (N), sulfur (S), or transition metals like iron (Fe) and tungsten (W), can substantially reduce TiO_2's bandgap, enhance visible-light absorption, and create additional active sites. Concurrently, the establishment of Z-scheme heterojunctions by combining two semiconductors with staggered band alignments can sustain robust redox potentials while promoting the separation of charge carriers. For instance, the combination of TiO_2 with g-C_3N_4 or $BiVO_4$ has demonstrated over a 200 % enhancement in H_2 yield in analogous photoreforming systems. The integration of such heterostructures with HPT-treated plastics may unveil new reaction pathways and extend light responsiveness. Moreover, surface plasmon-enhanced catalysts utilizing Ag or Au nanoparticles offer additional pathways for enhancing visible-light efficiency, particularly in low-intensity solar environments.

7.3 Reactor design: continuous-flow and solar-driven systems

The progression from batch-scale investigations to continuous, scalable reactor systems is critical for the practical deployment of this technology. Future reactor designs should prioritize continuous-flow photoreactors that facilitate a consistent input and output of plastic slurry and hydrogen gas, thereby enhancing process stability and scalability. Furthermore, the incorporation of solar concentrators or optical waveguides may significantly amplify solar light intensity and prolong photoreforming operations during fluctuating daylight scenarios. Innovations such as floating photocatalytic films or fluidized-bed reactor designs may further optimize light utilization and mass transfer. These advancements must be assessed not solely for hydrogen production efficiency but also for maintenance simplicity, catalyst recovery, and compatibility with HPT-treated feedstocks.[82]

7.4 Machine learning: AI-driven optimization of HPT and photoreforming

The intricate parameter landscape that regulates both HPT and photoreforming encompassing factors such as pressure, torsion velocity, catalyst loading, light intensity, and reaction duration constitutes an exemplary application for the deployment of machine learning (ML) and artificial intelligence (AI) methodologies. Predictive algorithms that are meticulously trained on empirical datasets possess the capability to discern optimal process parameters, thereby maximizing hydrogen output, minimizing energy expenditure, and regulating the formation of intermediates. Methodologies, including Gaussian Process Regression (GPR), Bayesian optimization, and neural networks, have already exhibited efficacy in the realm of materials science and could significantly expedite the development cycles associated with SPD-enabled catalysis. Furthermore, AI technologies may be employed for the real-time monitoring and regulation of reactor systems through image recognition, spectroscopic data analysis, and feedback-directed adjustments of processing parameters.[83]

7.5 Techno-economic analysis: lifecycle and scalability

To ascertain commercial feasibility, comprehensive techno-economic analysis (TEA) and LCA must be systematically incorporated into forthcoming research endeavors. These evaluations ought to consider the energy expenditures associated with HPT (e.g., approximately 0.3–0.5 kWh/kg of plastic), the synthesis of photocatalysts, the operation of reactors, and the purification of hydrogen. The lifecycle emissions stemming from HPT-photoreforming processes necessitate benchmarking against traditional waste treatment and hydrogen production methodologies, such as incineration or steam methane reforming. Preliminary TEA models indicate that, if appropriately scaled and integrated with cost-effective solar infrastructure, photoreforming could achieve levelized hydrogen production costs below $4/kg, thus positioning it competitively alongside green hydrogen standards. LCA findings have indicated potential GHG reductions of up to 3.2 tons CO_2-equivalent for every ton of plastic processed, making it an exceedingly appealing option for incorporation into circular economy frameworks.

7.6 Integration with circular economy: closing the loop

HPT-enhanced photoreforming possesses the potential to act as a fundamental technological component within circular economy models, facilitating not only hydrogen generation but also the recovery of valuable organic chemicals resulting from plastic degradation. Intermediates such as formic acid, acetic acid, and various short-chain carboxylic acids can be harvested and valorized as feedstocks for the chemical, pharmaceutical, or food sectors. Moreover, by synergistically linking photoreforming with waste sorting, solar energy harvesting, and fuel cell technologies, a comprehensive waste-to-energy cycle can be envisaged. Future investigative efforts should focus on decentralized circular systems, where plastic waste collected at the community level is converted into fuel and chemicals on-site, thereby eliminating the need for landfills. The establishment of policy frameworks and public-private partnerships will be pivotal in realizing these models at a significant scale.[84]

The prospective advancement of HPT-enhanced photoreforming relies on multidisciplinary collaboration spanning the fields of materials science, reactor engineering, data science, and circular economy strategy. Through coordinated initiatives across these domains, this pioneering approach holds the promise of evolving into a globally scalable solution for the valorization of plastic waste and the production of clean energy.

8 Conclusions

This comprehensive review elucidates the transformative potential inherent in combining HPT with photocatalytic

systems, aiming to achieve efficient solar-driven hydrogen production from polymeric waste materials. By interlinking diverse fields such as materials science, catalysis, and waste valorization, this investigation introduces an innovative framework for enhancing interactions between polymers and catalysts through the methodologies of defect engineering and interfacial optimization. Notably, this study repurposes HPT initially conceived as a metallurgical technique to induce surface and structural modifications that significantly enhance photocatalytic efficacy.

8.1 Key technical highlights

- **Defect Engineering:** The application of HPT facilitates grain refinement within the range of 50–200 nm, generates oxygen vacancies, and creates Ti^{3+} centers, thereby augmenting visible-light absorption and mitigating charge recombination phenomena.
- **Photocatalytic Yield:** The integration of brookite TiO_2 with HPT-modified PP yielded a remarkable 2.4-fold enhancement in hydrogen production, achieving levels of up to 580 $\mu mol\, h^{-1}\, g^{-1}$.
- **Reactive Intermediates:** The synthesis of organic acids at concentrations ranging from 50 to 200 $\mu mol\, L^{-1}$ markedly improved faradaic efficiency, surpassing 45 %.
- **Surface Enhancement:** Composites treated with HPT exhibited a reduction in contact angle by 30–40 % alongside a 40–60 % increase in BET surface area, thereby facilitating improved dispersion and charge transport dynamics.
- **Material Validation:** SEM, FTIR, Raman spectroscopy, and GC-MS corroborated significant morphological, chemical, and optical transformations consequent to HPT treatment.

8.2 Future outlook

The advancement of this hybrid methodology necessitates interdisciplinary research into co-doped photocatalysts, an expansion of compatible plastic feedstocks, and the incorporation of AI for real-time process control within continuous-flow reactors. Scaling the HPT-based photoreforming process within the framework of a circular economy could potentially reduce hydrogen production costs to below $4 per kilogram, while simultaneously decreasing CO_2 emissions by 3.2 tons for each ton of plastic processed. In summary, this approach presents a sustainable and highly efficient solution to the dual global challenges of plastic pollution and the generation of clean energy.

Research ethics: Not applicable.
Informed consent: Not applicable.
Author contributions: The authors have accepted responsibility for the entire content of this manuscript and approved its submission.
Use of Large Language Models, AI and Machine Learning Tools: Large Language Models, AI and Machine Learning Tools are not used.
Conflict of interest: The authors state no conflict of interest.
Research funding: None declared.
Data availability: Not applicable.

References

1. Alaghemandi, M. Sustainable Solutions through Innovative Plastic Waste Recycling Technologies. *Sustainability* **2024**, *16* (23), 10401.
2. Balu, R.; Dutta, N. K.; Choudhury, N. Plastic Waste Upcycling: A Sustainable Solution for Waste Management, Product Development, and Circular Economy. *Polymers* **2022**, *14* (22), 4788.
3. Phillip, A.; Chauhan, T. Innovative Biotechnological Approaches for Plastic Degradation: A Pathway to Sustainable Waste Management. *Int. J. Sci. Res. Arch.* **2024**, *13* (1), 2228–2243.
4. Elgarahy, A. M.; Priya, A. K.; Mostafa, H. Y.; Zaki, E. G.; El-Saeed, S. M.; Muruganandam, M.; Elwakeel, K. Z. Toward a Circular Economy: Investigating the Effectiveness of Different Plastic Waste Management Strategies: A Comprehensive Review. *J. Environ. Chem. Eng.* **2023**. https://doi.org/10.1016/j.jece.2023.110993.
5. D, C. S.; Channappagoudra, M.; Samantaray, S.; Mishra, A. K.; Juneja, G. Transforming Waste to Energy: Nanocatalyst Innovations Driving Green Hydrogen Production. *Rev. Inorg. Chem.* **2025**. https://doi.org/10.1515/revic-2025-0016.
6. Yi, X.; Qi, Y.; Li, F.; Shu, J.; Sun, Z.; Sun, S.; Pu, S. Effect of Electrolyte Reuse on Metal Recovery from Waste CPU Slots by Slurry Electrolysis. *Waste Manag.* **2019**, *95*, 370–376.
7. Li, R.; Wang, F.; Lv, F.; Wang, P.; Guo, X.; Chen, Y.; Li, D. Simultaneous Hydrogen Production and Conversion of Plastic Wastes into Valued Chemicals over a Z-Scheme Photocatalyst. *Int. J. Hydrogen Energy* **2023**. https://doi.org/10.1016/j.ijhydene.2023.10.069.
8. Edirisooriya, E. M. N.; Senanayake, P. S.; Xu, P.; Wang, H. Hydrogen Production and Value-Added Chemical Recovery from the Photo-Reforming Process Using Waste Plastics. *J. Environ. Chem. Eng.* **2023**. https://doi.org/10.1016/j.jece.2023.111429.
9. Nguyen, T. K. A.; Trần-Phú, T.; Daiyan, R.; Ta, X. M. C.; Amal, R.; Tricoli, A. From Plastic Waste to Green Hydrogen and Valuable Chemicals Using Sunlight and Water. *Angew. Chem.* **2024**. https://doi.org/10.1002/ange.202401746.
10. Bharvad, R. R.; Prajapati, N. H. Design and Analysis of High-Pressure Torsion Process Using Finite Element Method. *Int. J. Adv. Res. Sci. Commun. Technol.* **2023**, 331–345. https://doi.org/10.48175/ijarsct-13860.
11. Omranpour Shahreza, B.; Sergejev, F.; Ivanisenko, J.; Huot, J. A Promising Approach to Solid-State Hydrogen Storage: Mechanical Nanostructuring Synthesis of Magnesium by High Pressure Torsion Extrusion. *Adv. Sci. Technol.* 2023. https://doi.org/10.4028/p-4ccboq.

12. Miao, P.; Zhao, J.; Wang, P.; Shi, R.; Zhang, T. Enhanced Photocatalytic Hydrogen Production from Poly(vinyl Alcohol) Plastic-Dissolved Wastewater. *ACS Mater. Lett.* **2024**. https://doi.org/10.1021/acsmaterialslett.3c01573.
13. Ya, Z.; Tang, L.; Xu, D.; Wang, H.; Zhang, S. Photoreforming of Waste Plastic by B-doped Carbon Nitride Nanotube: Atomic-level Modulation and Mechanism Insights. *AIChE J.* **2025**. https://doi.org/10.1002/aic.18740.
14. Duan, F.; Chen, Y.; Chen, M.; Zhou, Y.; Shen, M.; Zhang, L.; Ren, S. Molecular Engineering of Covalent Organic Frameworks for Photocatalytic Hydrogen Evolution from Water. *Chemistry* **2024**, e202403627. https://doi.org/10.1002/chem.202403627.
15. Tang, Y.; Song, M.; Dong, J.; Li, G.; Ye, C.; Hu, Y.; Zheng, Y.; Wang, L. Synergetic Effect of In-Situ CaO on PVC Plastic Pyrolysis Characteristics: TG and Py GC/MS Analysis. *Polym. Degrad. Stabil.* **2025**, *234*, 111205.
16. Vámos, C.; Füredi, M.; Hórvölgyi, Z.; Krafcsik, O.; Kiss, G.; Bárány, T.; Marosfői, B. B. Analysis of Time-dependent Hydrophobic Recovery on Plasma-Treated Superhydrophobic Polypropylene Using XPS and Wettability Measurements. *Dent. Sci. Rep.* **2024**, *14* (1). https://doi.org/10.1038/s41598-024-72573-y.
17. Jeong, H. W.; Park, H.; Janáky, C. Developments in Nanostructuring for Enhanced Solar Water Splitting: Investigating Morphology Effects on Photoelectrode Performance. *Meet. Abstr.* 2024, *MA2024-02* (59), 3941.
18. Gao, X.; Chen, J.; Che, H.; Yang, H. B.; Liu, B.; Ao, Y. Accelerating Small Electron Polaron Dissociation and Hole Transfer at Solid–Liquid Interface for Enhanced Heterogeneous Photoreaction. *J. Am. Chem. Soc.* **2024**. https://doi.org/10.1021/jacs.4c11123.
19. Michelas, M.; Wimberger, L.; Boyer, C. A General Approach for Photo-Oxidative Degradation of Various Polymers. *Macromol. Rapid Commun.* **2024**. https://doi.org/10.1002/marc.202400358.
20. Oh, S.; Stache, E. E. Recent Advances in the Oxidative Degradation of Plastics. *Chem. Soc. Rev.* **2024**. https://doi.org/10.1039/d4cs00407h.
21. Vellaiyan, S. Synthesis and Characterisation of Waste-Derived Biodiesel and Enhancement of its Energy and Environmental Metrics Using Cetane Improver: an Experimental Study. *Int. J. Ambient Energy* **2024**, *45* (1). https://doi.org/10.1080/01430750.2024.2409825.
22. Kerketta, U.; Kim, H. W.; Denisov, N.; Schmuki, P. Grätzel-Type TiO_2 Anatase Layers as Host for Pt Single Atoms: Highly Efficient and Stable Photocatalytic Hydrogen Production. *Adv. Energy Mater.* **2023**. https://doi.org/10.1002/aenm.202302998.
23. Ma, L.; Fang, Z.; Duan, J.; Jin, L.; Zhu, K.; Jiang, Y.; Ji, B.; Yang, Z. Mesoporous TiO_2@g-C3n4 Nanostructure-Enhanced Photocatalytic Degradation of Tetracycline under Full-Spectrum Sunlight. *Molecules* **2024**, *29* (24), 5981.
24. Wang, S.; Li, Y.; Cheng, X.; Zhang, R.; Zhou, Q.; Xin, J.; Yan, D.; Xu, J.; Lu, X. Property of Waste Bottle-grade Polyethylene Terephthalate Restored by Ti-based Catalysts. *AIChE J.* **2024**. https://doi.org/10.1002/aic.18629.
25. Mortazavi Milani, H.; Van Neste, B.; Cosaert, E.; Poelman, D. Assessing the Stability and Photocatalytic Efficiency of a Biodegradable PLA-TiO_2 Membrane for Air Purification. *Adv. Sustain. Syst.* **2024**. https://doi.org/10.1002/adsu.202400594.
26. Nguyên, T. T.; Edalati, K. Brookite TiO_2 as an Active Photocatalyst for Photoconversion of Plastic Wastes to Acetic Acid and Simultaneous Hydrogen Production: Comparison with Anatase and Rutile. *Chemosphere* **2024**, *355*, 141785.
27. Mohammed Ajmal, S. F.; Natrayan, L.; Giri, J.; Makki, E.; Shah, M. A.; Mallik, S. Utilization of Response Surface Methodology to Optimize the Mechanical Behaviour of Flax/nano TiO_2/Epoxy Based Hybrid Composites under Liquid Nitrogen Environment. *Front. Mater.* **2024**, *11*. https://doi.org/10.3389/fmats.2024.1344351.
28. Žerjav, G.; Žižek, K.; Zavašnik, J.; Pintar, A. Brookite vs. Rutile vs. Anatase: What`s behind Their Various Photocatalytic Activities? *J. Environ. Chem. Eng.* **2022**, *10* (3), 107722.
29. D, C. S.; Devarajan, Y. , T. , R.; L, N. Green Hydrogen from Waste: Exploring the Promise of Sustainable Catalysis. *BioNanoScience* **2025**, *15* (3). https://doi.org/10.1007/s12668-025-02048-5.
30. Dong, J.; Tang, Y.; Hu, Y.; Wang, S.; Zhou, Z.; Shi, Y.; Wang, F. Effect of CaO Addition on Fast Pyrolysis Behavior of Solid Waste Components Using Py GC/MS. *J. Anal. Appl. Pyrolysis* **2025**, *188*, 107055.
31. Ziashahabi, A.; Poursalehi, R.; Naseri, N.; Peymani, R. Shed Light on Defect-Induced Enhanced Visible-Light Photocatalysis Activity of Rutile TiO_2 Nanoparticles: Effects of Annealing on Blue-Grey to Light-Grey Transition. *J. Mater. Res. Technol.* **2022**, *17*, 2400–2409.
32. Natrayan, L.; Janardhan, G.; Paramasivam, P.; Dhanasekaran, S. Enhancing Mechanical Performance of TiO2 Filler with Kevlar/epoxy-Based Hybrid Composites in a Cryogenic Environment: a Statistical Optimization Study Using RSM and ANN Methods. *Front. Mater.* **2023**, *10*. https://doi.org/10.3389/fmats.2023.1267514.
33. Christopher Selvam, D.; Devarajan, Y.; Raja, T.; Vickram, S. Advancements in Water Electrolysis Technologies and Enhanced Storage Solutions for Green Hydrogen Using Renewable Energy Sources. *Appl. Energy* **2025**, *390*, 125849.
34. Bott-Neto, J. L.; Martins, T. S.; Pimentel, G. J. C.; Oliveira, O. N.; Marken, F. Photoelectrochemical Performance of Brookite Titanium Dioxide Electrodeposited on Graphene Foam for Portable Biosensors. *ACS Omega* **2024**, *9* (52), 51474–51480.
35. Revenko, A. O.; Kozlov, D. A.; Kolesnik, I. V.; Poluboiarinov, A. S.; Kottsov, S. Y. U.; Garshev, A. V. Amorphous Titania as a Precursor to Brookite-Based Materials Obtained via Hydrothermal Treatment. *CrystEngComm* **2024**, *26* (37), 5152–5164.
36. Rad, S.; Gan, L.; Li, Z.; Dai, J.; Shahab, A. Review of the Sol–Gel Method in Preparing Nano TiO2 for Advanced Oxidation Process. *Nanotechnol. Rev.* **2023**. https://doi.org/10.1515/ntrev-2023-0150.
37. Zou, Y.; Yu, T.; Huang, X.-H.; Li, Y.; Guo, L.; Yan, H.; Zhou, J.; Wang, Y. H. Hydrothermal Synthesis of Zn-Doped Brookite TiO2 for Enhanced Visible-Light-Responsive Photocatalytic Performance. *Mater. Res. Express* **2023**, *10*. https://doi.org/10.1088/2053-1591/aceed4.
38. Vellaiyan, S. Development of Sustainable Diesel Fuel Blend Using Biodiesel, Hydrous Hydrazine and Nanocatalysts for Optimized Performance and Emission Control. *Case Stud. Therm. Eng.* **2025**, *69*, 105966.
39. Han, Q.; Wang, L.; Li, J.; Dong, Y.; Ma, Y.; ZhangYu, J. S. Built-in Field-Driven S-Scheme Boron-Doped nanodiamond/TiO2(101)/MXene Photocatalyst for Efficient Antibiotic Elimination: Mechanisms and DFT Validation. *Chem. Eng. J.* **2025**, *519*, 165290.
40. Jain, A.; Bora, B. J.; Kumar, R.; Paramasivam, P.; Lakshmaiya, N.; Kanti, P. K.; Dabelo, L. H. Conversion of Water Hyacinth Biomass to Biofuel with TiO_2 Nanoparticle Blending: Exergy and Statistical Analysis. *Case Stud. Therm. Eng.* **2025**, *67*, 105771.
41. Chen, L.; Wang, C.; Wang, Z.; Li, G. Pivotal Role of Water Vapor Mediated Defect Engineering on SrTiO3 Nanofiber toward Efficiency Photocatalytic Water Splitting. *Mater. Today Energy* **2024**, 101622. https://doi.org/10.1016/j.mtener.2024.101622.
42. Wu, C.; Song, K.; Zhang, X.; Tan, B.; Liao, R.; Liu, Z.; Zhu, H.; Wang, J. Highly Efficient Photocatalytic CO_2-to-CO on Ni-Based Cationic Polymer with TiO_2-Assisted Exfoliation and Stabilization. *Angew. Chem.* **2024**. https://doi.org/10.1002/anie.202423200.
43. Christopher Selvam, D.; Devarajan, Y. Bio-inspired Hybrid Materials for Sustainable Energy: Advancing Bioresource Technology and Efficiency. *Mater. Today Commun.* **2025**, *46*, 112647.

44. Tsuchiya, K. Grain Refinement in High-Entropy Alloys by High-Pressure Torsion Deformation. *Rev. High. Pres Sci. Technol.* **2022**, *32* (2), 64–70.
45. Zayed, E. M.; Shazly, M.; Elsabbagh, A.; El Mahallawy, N. Optimizing High-Pressure Sliding Process Parameters for Grain Refinement and Enhanced Mechanical Properties Using Response Surface Methodology Approach. *Discover Mech. Eng.* **2025**, *4* (1). https://doi.org/10.1007/s44245-025-00086-7.
46. Liu, Y. T.; Yu, J.; Wu, G.; Zhang, Z.; Lu, D.; Zhang, Z.; Huang, H.; Li, L. Grain Refinement Mechanism in Gradient Nanostructured Mg-Gd-Y-Zn-Zr Alloy Prepared by Severe Shear Deformation. *Mater. Sci. Eng. A Struct. Mater. Prop. Microstruct. Process.* **2024**. https://doi.org/10.1016/j.msea.2024.146207.
47. Vellaiyan, S. Greener Reprocessing of Medical Plastic Waste through Fuel Conversion and Enhancing its Energy and Environmental Metrics along with Economic Assessment. *J. Therm. Anal. Calorim.* **2025**, *150* (3), 1585–1598.
48. Figueiredo, R. B.; Kawasaki, M.; Langdon, T. G. The Role of Grain Size in Achieving Excellent Properties in Structural Materials. *J. Mater. Res. Technol.* **2024**. https://doi.org/10.1016/j.jmrt.2024.04.059.
49. Ohmura, T.; Wakeda, M. Nano Mechanical Characterization and Physical Modeling of Plastic Deformation Chapter 1: Dislocation-Grain Boundary Interaction as a Strengthening Factor. *J. Jpn. Inst. Metals* **2023**, *87* (2), 31–44.
50. Kuriachen, B. Influence of Surface Texture of Electric Discharge Machined Ti6Al4V on the Surface Wettability. *Precis. Eng.-J. Int. Soc. Precis. Eng. Nanotechnol.* **2024**. https://doi.org/10.1016/j.precisioneng.2023.12.016.
51. Ye, Q.; Li, X.; Zhang, W.; Xia, Y.; He, X.; Huang, H.; Gan, Y.; Xia, X.; Zhang, J. Slurry-Coated LiNi0.8Co0.1Mn0.1O2-Li3InCl6 Composite Cathode with Enhanced Interfacial Stability for Sulfide-Based All-Solid-State Batteries. *ACS Appl. Mater. Interfaces* **2023**, *15* (15), 18878–18888.
52. Varadarajan, S.; Kavitha, A.; Selvaraju, P.; Muthu, S. E.; Gurushankar, K.; Shanmugan, S.; Kannan, K. Enhanced Photocatalytic Hydrogen Evolution by TiO_2: A Synergistic Approach with Defect-Rich SnS2 and Ti_3C_2 MXene Cocatalysts. *Hydrogen* **2024**, *5* (4), 940–957.
53. Vellaiyan, S. Environmental Performance Improvement of Ammonium Hydroxide-Diesel Blends via Carbon Nanotube Catalysis and Electrostatic Nanoparticle Filtration. *J. Hazard Mater.* **2025**, *485*, 136906.
54. Das, D.; Shyam, S. Reduced Work Function in Anatase ⟨101⟩ TiO_2 Films Self-Doped by O-vacancy-dependent Ti^{3+} Bonds Controlling the Photocatalytic Dye Degradation Performance. *Langmuir* **2024**. https://doi.org/10.1021/acs.langmuir.4c00028.
55. Lazić, V.; Nedeljković, J. M. Photocatalytic Reactions over TiO_2-Based Interfacial Charge Transfer Complexes. *Catalysts* **2024**, *14* (11), 810.
56. Zajac, K.; Macyk, J.; Szajna, K.; Krok, F.; Macyk, W.; Kotarba, A. Functionalization of Polypropylene by TiO_2 Photocatalytic Nanoparticles: On the Importance of the Surface Oxygen Plasma Treatment. *Nanomaterials* **2024**, *14* (16), 1372.
57. Liang, X.; Ding, Y.; Cui, Y.; Dong, Q.; Li, X.; Labidi, A.; Lichtfouse, É.; Li, F.; Ye, F.; Wang, C. Photoreforming of Poly(ethylene-Terephthalate) Plastic into Valuable Chemicals and Hydrogen over BiVO4/MoOx: Synergistic Promotion of Oxidation and Reduction Processes. *Appl. Catal. B Environ.* **2024**, *357*, 124326.
58. Xiang, D.; Zhou, K.; Huang, J.; Kang, Q.; Li, H.; Duan, Y.; Du, J.; Hong, L. Electrochemical Upgrading of Waste Polylactic Acid Plastic for the Coproduction of C2 Chemicals and Green Hydrogen. *Molecules* **2024**, *29* (22), 5323.
59. Niu, Y.; Pan, F.; Shen, K.; Yang, X.; Niu, S.; Xu, X.; Zhou, H.; Fu, Q.; Li, X. Status and Enhancement Techniques of Plastic Waste Degradation in the Environment: A Review. *Sustainability* **2024**, *16* (21), 9395.
60. Chen, Q.; Yan, H.; Zhao, K.; Wang, S.; Zhang, D.; Li, Y.; Fan, R.; Li, J.; Chen, X.; Zhou, X.; Liu, Y.; Feng, X.; Chen, D.; Yang, C. Catalytic Oxidation Upcycling of Polyethylene Terephthalate to Commodity Carboxylic Acids. *Nat. Commun.* **2024**, *15* (1). https://doi.org/10.1038/s41467-024-54822-w.
61. Dileep, D.; Forrester, M.; Bonde, J.; Vega, V.; Burton, L. C.; Lee, T.; Ananin, A.; Kuehl, B.; Kraus, G. A.; Cochran, E. W. Not Cutting Corners: Bioderived Triggers Driving Oxidative Main Chain Scission of Poly(ethylene Terephthalate). *ACS Sustain. Chem. Eng.* **2024**, *12* (52), 18616–18623.
62. Bunke, S.; Yu, H.; Gil, H.; Tarpeh, W. A.; Kang, D. (Invited) Enhancing PET Plastic Circularity and Decarbonization through Process Electrification and Intensification. *Meet. Abstr.* 2024, *MA2024-02* (69), 4852.
63. Wang, Z.; Wang, Y.; Xiao, G.; Tang, Z.; Wang, S.; Jin, Y.; Su, H. Modular Chem-bio Upcycling of Waste Poly(ethylene Terephthalate) to Glycolic Acid and 2,4-pyridine Dicarboxylic Acid. *AIChE J.* **2024**. https://doi.org/10.1002/aic.18686.
64. Bhom, F.; Isa, Y. M. Photocatalytic Hydrogen Production Using TiO_2-based Catalysts: A Review. *Global Chall.* **2024**. https://doi.org/10.1002/gch2.202400134.
65. Ortiz, R. A.; Macías, R. Y.; Alfaro, K. G.; Delgado, V. J. C.; González, F. R.; Herrera, J. de J. K.; Valdez, A. E. G. Synthesis of Two TiO_2-Based Prodegradant Additives and Their Efficiency in Inducing the Accelerated Photo-Oxidation of Low-Density Polyethylene. *Polym. Degrad. Stabil.* **2024**. https://doi.org/10.1016/j.polymdegradstab.2024.110753.
66. Du, H.; Komuro, A.; Seki, Y.; Kobayashi, M.; Ono, R. Mechanism behind Polypropylene Surface Modifications by OH Radicals: An Experimental Study. *Appl. Surf. Sci.* **2023**. https://doi.org/10.1016/j.apsusc.2023.159086.
67. Anshari, R.; Tsuboi, M.; Sato, H.; Tashiro, K.; Ozaki, Y. Raman and ATR-FTIR Unmask Crystallinity Changes and Carboxylate Group and Vinyl Group Accumulation in Natural Weathering Polypropylene Microplastics. *Dent. Sci. Rep.* **2025**, *15* (1). https://doi.org/10.1038/s41598-025-85837-y.
68. Jia, W.; Yao, Y.; Guo, J.; Zhang, X.; Liang, Z. Study of the Surface Properties of Polypropylene by Enzyme Treatment. *Textil. Res. J.* **2022**, *93*, 2464–2472.
69. Tasbihi, M.; Kwon, S.; Kim, B.; Brüggemann, D.; Hou, H.; Lu, J.; Amitrano, R.; Grimm, T.; García-Antón, J.; Strasser, P.; Riedel, S. L.; Schwarze, M. Polyhydroxykanoate-Assisted Photocatalytic TiO_2 Films for Hydrogen Production. *Langmuir* **2024**. https://doi.org/10.1021/acs.langmuir.4c02727.
70. Jayabal, R. Environmental Impact of Adding Hybrid Nanoparticles and Hydrogen to the Algae Biodiesel-Diesel Blend on Engine Emissions. *Process Saf. Environ. Prot.* **2025**, *198*, 107102.
71. Shelake, S.; Sutar, D. N.; Abraham, B. M.; Banerjee, T.; Sainath, A. V.; Pal, U. Emerging Photoreforming Process to Hydrogen Production: A Future Energy. *Adv. Funct. Mater.* **2024**. https://doi.org/10.1002/adfm.202403795.
72. Damian, C. S.; Devarajan, Y.; Jayabal, R. A Comprehensive Review of the Resource Efficiency and Sustainability in Biofuel Production from Industrial and Agricultural Waste. *J. Mater. Cycles Waste Manag.* **2024**, *26* (3), 1264–1276.

73. Su, F.; Nguyen, P. T. T.; Ma, X.; Yan, N. Photorefinery of Biomass and Plastics to Renewable Chemicals Using Heterogeneous Catalysts. *Angew. Chem.* **2024**. https://doi.org/10.1002/ange.202408504.
74. Martín-Lara, M. A.; Moreno, R.; Blázquez, G.; Calero, M. Hydrogen Production Came from Catalytic Reforming of Volatiles Generated by Waste-Plastic Pyrolysis over Sepiolite-Based Catalysts. *Top. Catal.* **2024**. https://doi.org/10.1007/s11244-024-01981-1.
75. Greco-Coppi, M.; Eisenbach, N.; Kurkunc, M.-D.; Sattler, M.; Roloff, N.; Ströhle, J.; Epple, B. Carbon-Neutral Polygeneration in Waste-To-Energy Plants: Techno-Economic Study Using Carbon Capture and Utilization. *Soc. Sci. Res. Netw.* **2025**. https://doi.org/10.2139/ssrn.5069382.
76. Poorvashree, K. H.; Kalaivi, V.; Dharshan, S.; Kumari, K. A.; Anagha, H. M.; Kumar, N.; Menon, S. V.; Menon, S. V. Developing A Green and Sustainable Future: Advancements and Integration of Renewable Energy Resources. *J. Mod. Green Energy* **2024**, *3*, 7.
77. Zhao, H.; Zhao, X.; Zhang, J.; Anandita, S.; Liu, W.; Koh, S. W.; Yu, S.; Li, C.; Chen, Z.; Xu, R.; Zou, Z.; Tu, W.; Li, H. Solar-Driven Photoelectrochemical Upcycling of Polyimide Plastic Waste with Safe Green Hydrogen Generation. *Adv. Energy Mater.* **2024**. https://doi.org/10.1002/aenm.202400037.
78. Somadayo, S.; Supratman, S.; Hasanah, D.; Sutrisna Wp, A. G.; Agung, T. S. Innovative Waste-To-Energy Solutions: Assessing the Potential of Circular Economy Models for Sustainable Waste Management. *Global Int. J. Innov. Res.* **2024**, *2* (11). https://doi.org/10.59613/global.v2i11.351.
79. Schiavon, M.; Ravina, M.; Zanetti, M.; Panepinto, D. State-of-the-Art and Recent Advances in the Abatement of Gaseous Pollutants from Waste-To-Energy. *Energies* **2024**. https://doi.org/10.3390/en17030552.
80. Ayub, Y.; Ren, J. Revealing the Synergistic Effect of Feedstock Compositions and Process Parameters in Co-pyrolysis: A Review Based on Bibliometric Analysis and Experimental Studies. *J. Clean. Prod.* **2024**. https://doi.org/10.1016/j.jclepro.2024.142540.
81. Zhang, Q.; Ge, A.; Xiao, S.; Zhu, C.; Li, X.; Zhang, W.; An, C. Synergistic Enhancement of Photocatalytic Degradation of Polyethylene Plastics by Ni Cocatalyst and Oxygen Vacancies Engineering TiO_2 Nanosheets. *ChemistrySelect* **2025**, *10* (3). https://doi.org/10.1002/slct.202402265.
82. Creasey, G.; Moelich, A. W.; Acosta, J.; Shalvey, T. P.; Garcia-Osorio, D. A.; McCallum, T.; O'Neil, L.; Zhu, J.; Halder, S.; Ai, R.; Major, J. D.; Cowan, A. J.; McGregor, C.; Kafizas, A.; Kelsall, G. H. Up-Scaling Solar Hydrogen Production: Development and Demonstration of Photoelectrochemical Reactors. *Meet. Abstr.* 2024, *MA2024-02* (59), 3927.
83. Hamrani, A.; Medarametla, A.; John, D.; Agarwal, A. Machine-Learning-Driven Optimization of Cold Spray Process Parameters: Robust Inverse Analysis for Higher Deposition Efficiency. *Coatings* **2024**, *15* (1), 12.
84. Jiang Abudurexitia, A. S.; Abulikemu, Z.; Bavumiragira, J. P. Circular Economy and Sustainable Development Goals in the Reduction of Global Nano (Micro) Plastic Pollution. *Pol. J. Environ. Stud.* **2024**. https://doi.org/10.15244/pjoes/190280.